THE GEOLOGICAL SOCIETY OF AMERICA®

Triggering of volcanic degassing by large earthquakes

Dulcinea M. Avouris[1,2], Simon A. Carn[1], and Gregory P. Waite[1]
[1]Department of Geological and Mining Engineering and Sciences, Michigan Technological University, Houghton, Michigan 49931, USA
[2]Department of Geology, Kent State University, Kent, Ohio 44242, USA

ABSTRACT

Statistical analysis of temporal relationships between large earthquakes ($M_w \geq 7$) and volcanic eruptions suggests that seismic waves may trigger eruptions over great (>1000 km) distances from the epicenter, but a robust relationship between volcanic and teleseismic activity remains elusive. Here we investigate the relationship between dynamic stresses propagated by surface waves and a volcanic response, manifested by changes in sulfur dioxide (SO_2) emissions measured by the spaceborne Ozone Monitoring Instrument (OMI). Surface wave amplitudes for a catalog of 69 earthquakes in A.D. 2004–2010 are modeled at 12 persistently degassing volcanoes detected by the OMI. The volcanic response is assessed by examining daily OMI SO_2 measurements in 28 day windows centered on earthquakes meeting a variable peak dynamic stress threshold. A positive volcanic response is identified if the average post-earthquake SO_2 mass was at least 20% larger than the pre-earthquake SO_2 mass. We find two distinct volcanic responses, correlating strongly with eruption style. Open-vent, basaltic volcanoes exhibit a positive response to earthquake-generated dynamic stress (i.e., the earthquake triggers increased SO_2 discharge), and andesitic volcanoes exhibit a negative response. We suggest that the former is consistent with disruption or mobilization of bubbles, or magma sloshing, in low-viscosity magmas, whereas the latter observation may reflect more dominant controls on degassing in viscous magmas or a post-earthquake reduction in permeability. Overall this analysis suggests that the potential effects of large earthquakes should be taken into account when interpreting trends in volcanic gas emissions.

INTRODUCTION

The potential for triggering of volcanic activity by large earthquakes has been pondered for centuries: Pliny the Elder addressed the topic in A.D. 77–79 (Holland, 1601). Volcanic responses to earthquakes are difficult to quantify in a robust manner, however, largely because only a small proportion of global volcanoes are adequately monitored. Despite this, there is mounting evidence for earthquake-triggered volcanic activity on various time scales (e.g., Linde and Sacks, 1998; Brodsky et al., 1998; Manga and Brodsky, 2006; Cigolini et al., 2007; Harris and Ripepe, 2007; Walter and Amelung, 2007; Walter et al., 2007; Watt et al., 2009; De la Cruz-Reyna et al., 2010; Delle Donne et al., 2010). Some of these studies have been catalyzed by decade-scale satellite remote sensing observations of volcanic activity (e.g., Delle Donne et al., 2010). Quantitative measurements of changes in both the earthquake-generated state of stress and volcanic activity (including ground deformation, heat flux, and degassing) may provide greater insight into the triggering mechanism as well as the types of volcanoes that may be susceptible to triggering. However, to date there has been no analysis of the volcanic response to earthquakes based on direct observations of volcanic degassing.

Here we assess the links between volcanic degassing and dynamic (not static) stresses propagated by large earthquakes by modeling surface wave propagation from M7 and greater earthquakes in 2004–2010 to a selection of target volcanoes with sulfur dioxide (SO_2) emissions measurable by satellite remote sensing. Surface wave modeling and the associated peak dynamic stress (PDS) calculations provide a robust method for identifying the earthquakes most likely to trigger a change in volcanic activity. SO_2 is the optimal indicator of volcanic degassing because it is easily distinguishable against the atmospheric background; for this reason it is the most commonly measured volcanic gas, and thus it is also crucial to understand processes that modulate its emission. We use daily measurements of volcanic SO_2 emissions from the Ozone Monitoring Instrument (OMI) on the NASA Aura satellite (Carn et al., 2013) that provide a consistent measure of volcanic degassing to compare with calculated PDS. The availability of daily satellite measurements of volcanic SO_2 emissions permits such an analysis on a large scale for the first time.

DATA AND METHODS

To quantify daily volcanic SO_2 emissions, we use the operational OMI SO_2 product derived using the linear fit algorithm (Level 2 OMSO2 data product; Yang et al., 2007), obtained from the NASA Goddard Earth Sciences Data and Information Services Center (DISC; http://disc.sci.gsfc.nasa.gov/). We selected the following target volcanoes, covering a variety of eruption styles in diverse arc settings, from those with SO_2 emissions detectable by OMI (e.g., Carn et al., 2017): Ambrym and Gaua (Vanuatu); Bagana, Rabaul, and Ulawun (Papua New Guinea); Fuego and Pacaya (Guatemala); Merapi, Semeru, and Bromo (Indonesia); Turrialba (Costa Rica); and Villarrica (Chile) (Table DR1 in the GSA Data Repository[1]). These volcanoes were all in an open-vent state in 2004–2010 (i.e., with a magma-atmosphere interface at or close to the surface), and therefore may be more sensitive to small earthquake-induced pressure changes. The eruptive styles represented range from active lava lakes (e.g., Ambrym, Villarrica) to open-vent degassing (e.g., Turrialba, Ulawun) to lava dome growth (e.g., Merapi, Semeru, Bagana).

For each target, we created a time series of daily SO_2 loading measured by OMI between 1 October 2004 and 30 September 2010 (e.g., Fig. 1). Volcanic plume altitude affects the OMI SO_2 retrievals (Yang et al., 2007), and so OMSO2 products are provided for several assumed altitudes (Carn et al., 2013), including lower troposphere (~3 km altitude) and mid-troposphere (~8 km). For plumes with a designated altitude in the Smithsonian Institution volcanic activity reports (Global Volcanism Program; Venzke, 2013), the OMSO2 product closest to the reported altitude was used. In all other cases the lower troposphere SO_2 product was used, assuming that passively degassed SO_2 would rise no higher than 3–4 km at the target volcanoes. Daily SO_2 loading was calculated for each target volcano in a 2° × 2° region centered on the vent. Where the 2° × 2° regions for 2 or more volcanoes overlapped, a larger box was established with boundaries 1° from the edges of the volcano cluster. This resulted in the clustering of Ambrym and Gaua (Fig. 1), Rabaul and Ulawun, Fuego and Pacaya; and Merapi, Semeru, and Bromo; in these cases multiple sources of SO_2 degassing were considered as a single source. However, recent work (Carn et al., 2017) indicates that the dominant SO_2 sources in these regions are Ambrym, Rabaul, Fuego, and Semeru-Bromo (emissions from the latter are essentially indistinguishable in

[1]GSA Data Repository item 2017230, additional results, Tables DR1–DR9, and Figures DR1and DR2, is available online at http://www.geosociety.org/datarepository/2017/ or on request from editing@geosociety.org.

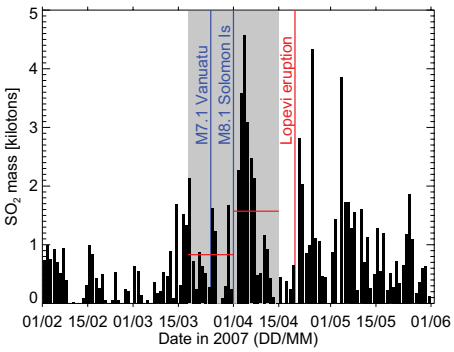

Figure 1. Example of pre-earthquake and post-earthquake window analysis using a time series of daily spaceborne Ozone Monitoring Instrument SO_2 measurements (black bars) at Ambrym-Gaua (Vanuatu), from 1 February to 1 June 2007. Two major regional earthquakes occurred in this period: a M_w 7.1 event in Vanuatu on 25 March and an M_w 8.1 event in the Solomon Islands (~1500 km from Ambrym) on 1 April (blue lines). The gray shading indicates the 14 day pre-earthquake and post-earthquake time windows in which daily SO_2 loadings were averaged for the M_w 8.1 Solomon Islands earthquake; horizontal red lines indicate the corresponding average SO_2 loadings in the two windows, showing higher SO_2 after the earthquake. We also note that Lopevi (south of Ambrym) erupted on 20 April 2007. Lopevi was not included in our analysis, but its eruption soon after two large regional earthquakes is an interesting coincidence.

satellite data), respectively. The daily SO_2 mass was smoothed using a 1 week moving average to mitigate the impact of daily variations in OMI viewing geometry (e.g., Flower et al., 2016), and OMI ultraviolet reflectivity data were also used to screen excessively cloudy SO_2 observations.

Our earthquake catalog (69 events) was derived from the U.S. Geological Survey global catalog (https://earthquake.usgs.gov/earthquakes/search/), and includes all moment magnitude (M_w) ≥ 7 earthquakes at depths of ≤35 km between 1 January 2004 and 30 September 2010 (Table DR2 in the GSA Data Repository). In addition, all M_w ≥ 8 events during the period are included, regardless of depth. We use Computer Programs in Seismology (CPS; Herrmann, 2013) to model surface wave amplitudes. CPS produces synthetic seismograms based on a layered Earth velocity model (ak135-F, http://ds.iris.edu/ds/products/emc-ak135-f/), the focal mechanism, depth, and M_w of the earthquake, and incorporates the distance and azimuth of the target from the epicenter. To validate our synthetic waveform data set, we compared a subset of synthetic seismograms to real data at a variety of azimuths and distances. We found that surface wave amplitudes in the synthetic seismograms were typically within a factor of 2–3 of the real data, consistent with other studies (e.g., van der Lee, 1998). Although our modeling was relatively simple and did not account for finite fault complexity (i.e., directivity), we do not feel that more sophisticated modeling would significantly improve the discrepancy between the synthetic and real seismograms.

Synthetic seismograms were computed for each earthquake in our catalog, using the target volcano locations as receiver positions. We used the synthetic seismograms to estimate the PDS with the simplified shear-wave method of Velasco et al. (2004):

$$\mathrm{PDS} = v\mu / \beta, \quad (1)$$

where v is ground velocity, μ is rigidity, and β is shear wave velocity. We used average crustal values of 3.3×10^{10} Pa for μ and 3.5 km/s for β (Velasco et al., 2004). Rather than calculate separate PDS for Rayleigh and Love waves, the three components of each synthetic seismogram were combined into a single velocity vector, from which peak velocity was derived for the time period spanning the arrivals of 40 s to 15 s period waves. Clearly our method does not properly account for Rayleigh wave PDS, but serves as a quantitative proxy for total surface wave PDS.

The OMI-derived SO_2 mass was averaged in two 14 day windows, one preceding and one following each earthquake, including the day of the event (e.g., Fig. 1). For each earthquake, the ratio of post-earthquake average SO_2 mass to pre-earthquake average SO_2 mass was calculated. The relationship between earthquake occurrence and SO_2 mass ratio was evaluated with variable thresholds of 1.2–2.0 (Tables DR3–DR9). The inverse of each SO_2 mass ratio was also calculated, to investigate if the PDS changes caused a decrease in volcanic degassing (i.e., a negative response). These calculations were repeated for PDS from 5 to 100 kPa, to investigate the effect of different levels of dynamic stress. To minimize the influence of meteorological clouds on the SO_2 data, we rejected days with a scene average reflectivity value >35%; in addition, if fewer than 8 days in either window met the reflectivity criterion, the earthquake was rejected.

In order to compare the occurrence of positive response to an earthquake to coincidental occurrence of elevated SO_2 emissions, we repeated the same windowing analysis for each day of the study period. This revealed any notable deviation in occurrence of response to an earthquake from that expected from random coincidence. We also further examined the variation in SO_2 response of two volcano clusters (Ambrym-Gaua and Merapi-Semeru-Bromo) by stacking the SO_2 emissions in a 31 day window centered on each qualifying earthquake generating PDS > 5 kPa. This provides a visualization of SO_2 degassing patterns before and after each earthquake and reveals how degassing re-equilibrates after an earthquake.

RESULTS AND DISCUSSION

PDS values calculated using modeled seismograms contain more useful information than moment magnitude because the effects of focal mechanism and distance are included. For example, there are instances where the PDS generated by a smaller earthquake is higher for specific volcanoes than the PDS generated by a larger earthquake (e.g., Fig. DR1). Notably, an M_w 7.3 event generated a higher PDS than all other earthquakes up to M_w 8.0 (Fig. DR1). Full results of the 14 day SO_2 data window analysis for each target volcano or volcano cluster are reported in Tables DR3–DR9, and summarized in Figure 2.

There are at least two challenges to assessing the volcanic degassing response to earthquakes with our method: the frequency of major earthquakes at shallow depths is relatively low, and we expect any SO_2 degassing response to be modest and so not always detectable from space. However, considering our target volcanoes as an ensemble, two robust results emerge (Fig. 2): open-vent basaltic volcanoes show a clear occurrence of elevated SO_2 output following earthquakes that generated high PDS (positive response; e.g., Ambrym, Villarrica), and volcanoes undergoing cyclic activity that may

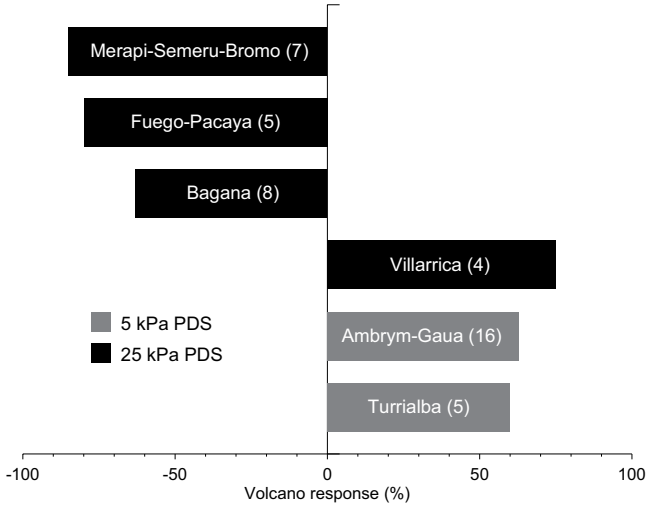

Figure 2. Volcano response to earthquake peak dynamic stress (PDS) at the 1.2 SO_2 mass ratio level, indicating the percentage of positive or negative response to earthquake PDS at 5 kPa and 25 kPa threshold levels. The number of earthquakes above the PDS threshold at each volcano is given in parentheses (Tables DR3–DR [see footnote 1]). We observe a clear dependence of response on eruptive style: volcanoes with plugged conduits show a negative response, whereas low-viscosity volcanic systems show a positive response.

include conduit plugging by more viscous magmas seem to demonstrate reduced SO_2 degassing following such earthquakes (negative response; e.g., Merapi, Fuego, Bagana). In this study, only Rabaul-Ulawun did not show a measurable degassing response to earthquake-induced dynamic stress; this could provide insight into the state of their magmatic plumbing systems.

Here we focus on our most significant results, i.e., the positive response of Ambrym-Gaua and the negative response of Merapi-Semeru-Bromo (Fig. 2). Ambrym-Gaua showed increased SO_2 emissions following 63% of earthquakes generating PDS of at least 5 kPa (Fig. 2), whereas higher SO_2 would be expected following only 41% of days selected at random. A stacked SO_2 emission plot (Fig. 3) indicates that SO_2 degassing at Ambrym (the dominant SO_2 source) consistently increased in response to earthquake-generated PDS. Ambrym hosted at least one active lava lake during the study period, likely maintained by the convection of low-viscosity basalt within the lake and conduit, driven by degassing-induced density variations (e.g., Stevenson and Blake, 1998). This suggests that a steady-state volcanic system that can maintain active lava lakes is more easily perturbed by small dynamic stresses (5 kPa; Fig. 3), and that the system responds by degassing SO_2 as it re-equilibrates.

Given that our calculated PDS values are likely far below the supersaturation pressures required for bubble nucleation (a few MPa in silicic magmas; e.g., Hurwitz and Navon, 1994), possible mechanisms to explain earthquake-triggered degassing include rectified diffusion (pumping of gas into preexisting bubbles; e.g., Brodsky et al., 1998) or sloshing (or another mass redistribution process) in a bubbly magma body (e.g., Carbone et al., 2009; Namiki et al., 2016). Disregarding rectified diffusion as inefficient (e.g., Ichihara and Brodsky, 2006), and given that the estimated PDS is commensurate with the stresses expected to weaken crystal-rich magma (e.g., Sumita and Manga, 2008), we favor a scenario whereby pockets of accumulated bubbles in the plumbing system are disrupted by dynamic strains, either mobilizing bubbles or increasing permeability via bubble wall collapse. Stacked plots of SO_2 emissions (Fig. 3A) indicate that peak SO_2 degassing occurs after a few days, suggesting that SO_2 release at the surface lags behind the triggering event (however, we have no constraints on the behavior of other volatiles, e.g., H_2O).

Merapi-Semeru-Bromo exhibited a negative response at all PDS levels (e.g., Fig. 2). This suggests minimal susceptibility to the effect of dynamic stress, at least with respect to degassing activity detectable from space. Figure 3B indicates a consistent decrease in degassing following each earthquake, with small post-event spikes that are less than pre-earthquake SO_2 emissions. We attribute this to the influence of higher viscosity basaltic-andesite or andesite magmas at these volcanoes, which typically erupt lava domes. In such systems, bubble rise is inhibited and degassing occurs primarily along permeable fracture networks in the conduit (e.g., Edmonds et al., 2003). Earthquake-induced stresses could act to modify or close existing fractures, reducing SO_2 emissions until the degassing pathway is reestablished. The cyclic nature of many dome-forming eruptions (e.g., Melnik and Sparks, 2005) may also be a dominant control on degassing, rendering them less susceptible to earthquake-induced effects. It is notable that Bebbington and Marzocchi (2011) found no statistical evidence for significant earthquake triggering of eruptions at Merapi, Semeru, or Bromo.

The earthquake sample size was lower for our other target volcanoes (Tables DR3–DR9), but the results concur with our proposed interpretation. Villarrica hosts an active lava lake and shows a positive degassing response (Fig. 2). Persistent, open-vent SO_2 emissions at Turrialba (e.g., Campion et al., 2012), coupled with its positive response, point to the involvement of low-viscosity magma supplying the emitted gases. This demonstrates the insight into volcanic systems that analysis of their response to earthquakes can yield.

Negative responses similar to Merapi-Semeru-Bromo were also observed at Fuego-Pacaya and Bagana (Fig. 2). The near-surface viscosity of conduit plugs and lavas likely exerts a strong control on activity at both Fuego and Bagana (e.g., Lyons et al., 2009; McCormick et al., 2012), with permeability governed by transient pore networks and cracks that could be susceptible to dynamic stresses (e.g., Heap and Kennedy, 2016). Thus in these cases permeability controls on degassing are likely dominant. The only neutral result in our analysis was found at Rabaul-Ulawun, which displayed no clear degassing response. There are many possible reasons for this, including opposing responses at each volcano (canceling out any net degassing signal), or the effects of static stress changes or fault rupture directivity (e.g., Delle Donne et al., 2010).

Our results indicate a striking dependence of the volcanic degassing response to earthquake-induced stresses on magma viscosity and eruptive style. We therefore recommend that interpretation of SO_2 emission time series at actively degassing volcanoes takes into account the potential effects of large earthquakes on observed trends. More significant insights into the nature of volcanic responses to earthquake-induced stresses are sure to arise from the coming years of observations of volcanic activity from space.

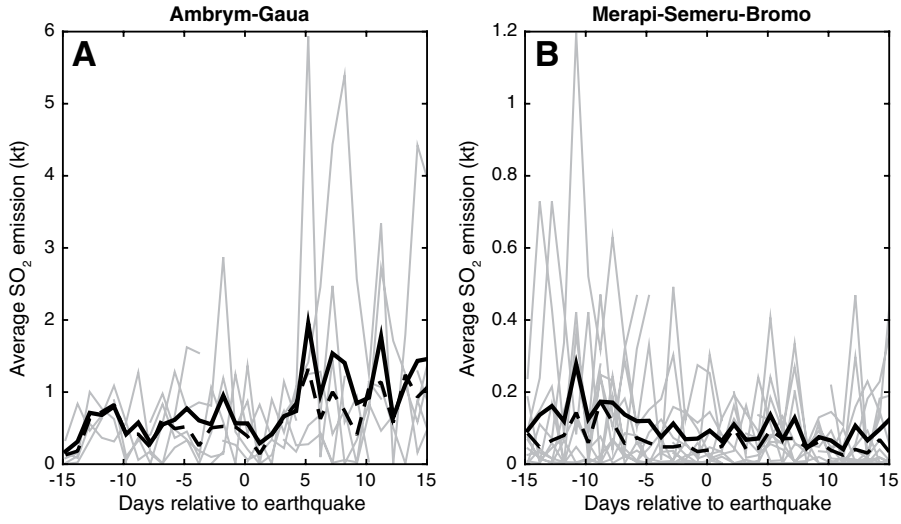

Figure 3. Stacked SO_2 emission time series covering 15 days before and after earthquakes that produced estimated peak dynamic stress (PDS) of at least 5 kPa at 2 volcano clusters. A: Ambrym-Gaua (Vanuatu). B: Merapi-Semeru-Bromo (Indonesia). Each plot shows the mean (bold line), median (dashed line), and individual time series (gray lines). In addition to the PDS calculation, the number of time series varies depending on availability of SO_2 data: 6 (A) and 13 (B). At Ambrym and Gaua, the results suggest a delayed increase in SO_2 emissions beginning ~5 d after an earthquake. Conversely, at Merapi-Semeru-Bromo, SO_2 emissions appear to decrease following earthquakes. Figure DR2 (see footnote 1) shows the same plot for a PDS of at least 25 kPa.

ACKNOWLEDGMENTS

We acknowledge R. Hermann for his help with the CPS (Computer Programs in Seismology) code. Ben Kennedy and Michael Manga provided constructive reviews that greatly improved the paper. This work was supported by the Michigan Space Grant Consortium (Avouris) and NASA (Aura Science Team grant NNX11AF42G and MEaSUREs grant NNX13AF50G to Carn).

REFERENCES CITED

Bebbington, M.S., and Marzocchi, W., 2011, Stochastic models for earthquake triggering of volcanic eruptions: Journal of Geophysical Research, v. 116, B05204, doi:10.1029/2010JB008114.

Brodsky, E.E., Sturtevant, B., and Kanamori, H., 1998, Earthquakes, volcanoes, and rectified diffusion: Journal of Geophysical Research, v. 103, p. 23,827–23,838, doi:10.1029/98JB02130.

Campion, R., Martinez-Cruz, M., Lecoq, T., Caudron, C., Pacheco, J., Pinardi, G., Hermans, C., Carn, S., and Bernard, A., 2012, Space- and ground-based measurements of sulphur dioxide emissions from Turrialba Volcano (Costa Rica): Bulletin of Volcanology, v. 74, p. 1757–1770, doi:10.1007/s00445-012-0631-z.

Carbone, D., Jousset, P., and Musumeci, C., 2009, Gravity 'steps' at Mt. Etna volcano (Italy): Instrumental effects or evidences of earthquake-triggered magma density changes?: Geophysical Research Letters, v. 36, L02301, doi:10.1029/2008GL036179.

Carn, S.A., Krotkov, N.A., Yang, K., and Krueger, A.J., 2013, Measuring global volcanic degassing with the Ozone Monitoring Instrument (OMI), *in* Pyle, D.M., et al., eds., Remote sensing of volcanoes and volcanic processes: Integrating observation and modeling: Geological Society of London Special Publication 380, p. 229–257, doi:10.1144/SP380.12.

Carn, S.A., Fioletov, V., McLinden, C.A., Li, C., and Krotkov, N.A., 2017, A decade of global volcanic SO_2 emissions measured from space: Scientific Reports, v. 7, 44095, p. 1–12, doi:10.1038/srep44095.

Cigolini, C., Laiolo, M., and Coppola, D., 2007, Earthquake-volcano interactions detected from radon degassing at Stromboli (Italy): Earth and Planetary Science Letters, v. 257, p. 511–525, doi:10.1016/j.epsl.2007.03.022.

De la Cruz-Reyna, S., Tárraga, M., Ortiz, R., and Martínez-Bringas, A., 2010, Tectonic earthquakes triggering volcanic seismicity and eruptions. Case studies at Tungurahua and Popocatépetl volcanoes: Journal of Volcanology and Geothermal Research, v. 193, p. 37–48, doi:10.1016/j.jvolgeores.2010.03.005.

Delle Donne, D., Harris, A.J.L., Ripepe, M., and Wright, R., 2010, Earthquake-induced thermal anomalies at active volcanoes: Geology, v. 38, p. 771–774, doi:10.1130/G30984.1.

Edmonds, M., Oppenheimer, C., Pyle, D.M., Herd, R.A., and Thompson, G., 2003, SO_2 emissions from Soufrière Hills Volcano and their relationship to conduit permeability, hydrothermal interaction and degassing regime: Journal of Volcanology and Geothermal Research, v. 124, p. 23–43, doi:10.1016/S0377-0273(03)00041-6.

Flower, V.J.B., Carn, S.A., and Wright, R., 2016, The impact of satellite sensor viewing geometry on time-series analysis of volcanic emissions: Remote Sensing of Environment, v. 183, p. 282–293, doi:10.1016/j.rse.2016.05.022.

Harris, A.J.L., and Ripepe, M., 2007, Regional earthquake as a trigger for enhanced volcanic activity: Evidence from MODIS thermal data: Geophysical Research Letters, v. 34, L02304, doi:10.1029/2006GL028251.

Heap, M.J., and Kennedy, B.M., 2016, Exploring the scale-dependent permeability of fractured andesite: Earth and Planetary Science Letters, v. 447, p. 139–150, doi:10.1016/j.epsl.2016.05.004.

Herrmann, R.B., 2013, Computer programs in seismology: An evolving tool for instruction and research: Seismological Research Letters, v. 84, p. 1081–1088, doi:10.1785/0220110096.

Holland, P., translator, 1601, The historie of the world, commonly called, The naturall historie of C. Plinius Secundus: London, A. Islip, p. 1–49: http://penelope.uchicago.edu/holland/index.html (accessed March 2017).

Hurwitz, S., and Navon, O., 1994, Bubble nucleation in rhyolitic melts: Experiments at high pressure, temperature, and water content: Earth and Planetary Science Letters, v. 122, p. 267–280, doi:10.1016/0012-821X(94)90001-9.

Ichihara, M., and Brodsky, E.E., 2006, A limit on the effect of rectified diffusion in volcanic systems: Geophysical Research Letters, v. 33, L02316, doi:10.1029/2005GL024753.

Linde, A.T., and Sacks, I.S., 1998, Triggering of volcanic eruptions: Nature, v. 395, p. 888–890, doi:10.1038/27650.

Lyons, J.J., Waite, G.P., Rose, W.I., and Chigna, G., 2009, Patterns in open vent, Strombolian behavior at Fuego volcano, Guatemala, 2005–2007: Bulletin of Volcanology, v. 72, p. 1–15, doi:10.1007/s00445-009-0305-7.

Manga, M., and Brodsky, E., 2006, Seismic triggering of eruptions in the far field: Volcanoes and geysers: Annual Review of Earth and Planetary Sciences, v. 34, p. 263–291, doi:10.1146/annurev.earth.34.031405.125125.

McCormick, B.T., Edmonds, M., Mather, T.A., and Carn, S.A., 2012, First synoptic analysis of volcanic degassing in Papua New Guinea: Geochemistry, Geophysics, Geosystems, v. 13, Q03008, doi:10.1029/2011GC003945.

Melnik, O., and Sparks, R.S.J., 2005, Controls on conduit magma flow dynamics during lava dome building eruptions: Journal of Geophysical Research, v. 110, B02209, doi:10.1029/2004JB003183.

Namiki, A., Rivalta, E., Woith, H., and Walter, T.R., 2016, Sloshing of a bubbly magma reservoir as a mechanism of triggered eruptions: Journal of Volcanology and Geothermal Research, v. 320, p. 156–171, doi:10.1016/j.jvolgeores.2016.03.010.

Stevenson, D.S., and Blake, S., 1998, Modelling the dynamics and thermodynamics of volcanic degassing: Bulletin of Volcanology, v. 60, p. 307–317, doi:10.1007/s004450050234.

Sumita, I., and Manga, M., 2008, Suspension rheology under oscillatory shear and its geophysical implications: Earth and Planetary Science Letters, v. 269, p. 468–477, doi:10.1016/j.epsl.2008.02.043.

van der Lee, S., 1998, Observations and origin of Rayleigh-wave amplitude anomalies: Geophysical Journal International, v. 135, p. 691–699, doi:10.1046/j.1365-246x.1998.00678.x.

Velasco, A.A., Ammon, C.J., Farrell, J., and Pankow, K., 2004, Rupture directivity of the 3 November 2002 Denali fault earthquake determined from surface waves: Seismological Society of America Bulletin, v. 94, p. S293–S299, doi:10.1785/0120040624.

Venzke, E., ed., 2013, Volcanoes of the World, v. 4.5.0: Washington, D.C., Smithsonian Institution Global Volcanism Program, doi:10.5479/si.GVP.VOTW4-2013 (accessed 22 August 2016).

Walter, T.R., and Amelung, F., 2007, Volcanic eruptions following M ≥ 9 megathrust earthquakes: Implications for the Sumatra-Andaman volcanoes: Geology, v. 35, p. 539–542, doi:10.1130/G23429A.1.

Walter, T.R., Wang, R., Zimmer, M., Grosser, H., Lühr, B., and Ratdomopurbo, A., 2007, Volcanic activity influenced by tectonic earthquakes: Static and dynamic stress triggering at Mt. Merapi: Geophysical Research Letters, v. 34, L05304, doi:10.1029/2006GL028710.

Watt, S., Pyle, D.M., and Mather, T.A., 2009, The influence of great earthquakes on volcanic eruption rate along the Chilean subduction zone: Earth and Planetary Science Letters, v. 277, p. 399–407, doi:10.1016/j.epsl.2008.11.005.

Yang, K., Krotkov, N.A., Krueger, A.J., Carn, S.A., Bhartia, P.K., and Levelt, P.F., 2007, Retrieval of large volcanic SO_2 columns from the Aura ozone monitoring instrument: Comparison and limitations: Journal of Geophysical Research, v. 112, D24S43, doi:10.1029/2007JD008825.

Manuscript received 17 February 2017
Revised manuscript received 2 April 2017
Manuscript accepted 19 April 2017

Printed in USA